Advanced Physical Research
Vol.7, No.3, 2025, pp.174-188
https://doi.org/10.62476/apr.73174

# PREPARATION OF SOLID SOLUTIONS IN $GeSb_4Te_7$ – $MnSb_4Te_7$ SYSTEM AND MAGNETIC PROPERTIES OF $Mn_{0.5}Ge_{0.5}Sb_4Te_7$

**Fuad Safarov**[1,2,3*], **Dunya Babanly**[1,2,4], **Leman Mahmudova**[2], **Murad Khalilzade**[5], **Elnur Orujlu**[1]

[1]Azerbaijan State Oil and Industry University (ASOIU), Baku, Azerbaijan
[2]French-Azerbaijani University (UFAZ), Baku, Azerbaijan
[3]Strasbourg Institute of Material Physics and Chemistry, Strasbourg, France
[4]Institute of Catalysis and Inorganic Chemistry (ICIC), Azerbaijan National Academy of Sciences (ANAS), Baku, Azerbaijan
[5]Chemistry-biology oriented Republican lyceum, Baku, Azerbaijan

**Abstract.** The rich surface-state physics of topological insulators underscores the importance of tuning their properties and developing efficient compounds. Motivated by the pressure-dependent superconductivity of $GeSb_4Te_7$ and $MnSb_4Te_7$, and the antiferromagnetism of the latter, we report the synthesis of $GeSb_4Te_7$–$MnSb_4Te_7$ solid solutions, enabled by their structural similarity and the comparable ionic radii of $Mn^{2+}$ and $Ge^{2+}$. As it was shown by PXRD analyses that around ∼50 % solubility of Mn at Ge sites in $GeSb_4Te_7$ was successfully achieved, while compositions with higher Mn substitutions (70% and 90%) and pristine $MnSb_4Te_7$ formed multiphasic mixtures consisting of phases based on $GeSb_4Te_7$, $MnSb_2Te_4$, and $Sb_2Te_3$. Le Bail analysis revealed that lattice parameter $a$ increases almost linearly with increasing Mn content, while lattice parameter $c$ decreases almost linearly - a trend that is unexpected, but consistent with observations in the Bi-based sister system. The middle range 50 % Mn substitution compound was selected for SQUID magnetometry, revealing two magnetic transitions at 14.4 K and 3.6 K, which correspond to paramagnetic-to-ferrimagnetic and ferrimagnetic-to-ferromagnetic transitions, respectively. Both effective and saturation magnetic moments decreased significantly compared to pristine $MnSb_4Te_7$, due to magnetic dilution from Ge ions and Mn ions present at Sb sites, both of which induce intralayer antiferromagnetic coupling. These findings facilitate the selection of compositions for single-crystal growth and subsequent investigations of magneto-transport properties and topological surface states.

**Keywords**: topological insulator, solid solution, PXRD, Le Bail analysis, SQUID magnetometry, ferrimagnetism.
**Corresponding author:** Fuad Safarov, Azerbaijan State Oil and Industry University (ASOIU), 34 Azadliq ave., AZ1010, Baku, Azerbaijan, e-mail: *fuad.safarov@ipcms.unistra.fr*
*Received: 25 July 2025; Revised: 28 August 2025; Accepted: 5 September 2025; Published: 16 October 2025.*

## 1 Introduction

Layered van der Waals (vdW) materials offer a powerful platform for exploring quantum phenomena due to their reduced dimensionality, tunable interlayer interactions, and ease of exfoliation to the monolayer limit. Their weakly bonded atomic layers enable the construction of custom heterostructures via stacking or epitaxial growth, allowing fine control over electronic, optical, and magnetic properties (Novoselov et al., 2004; Geim & Grigorieva, 2013). Among them, topological materials are notable for robust surface or edge states protected by the nontrivial topology of the bulk band structure.

The interplay between topology and magnetism in vdW systems has gained attention with the emergence of magnetic topological insulators (MTIs), which combine bulk insulating behavior with magnetic order – introduced through doping or intrinsic magnetism (Yu et al., 2010; Otrokov et al., 2019; Deng et al., 2020). MTIs exhibit quantum phenomena such as the quantum anomalous Hall effect, axion electrodynamics, and magnetoelectric coupling, making them attractive for spintronic and quantum technologies (Chang et al., 2013; Tokura et al., 2019).

The layered magnetic vdW $(MnSb_2Te_4)_m(Sb_2Te_3)_n$ family, as the sister system of $(MnBi_2Te_4)_m$ $(Bi_2Te_3)_n$ homologous series, also exhibits both versatile magnetism and band topology that are tunable from AFM topological insulator to FM Weyl semimetal state by carrier doping and magnetic field, though its members remain much less explored (Huan et al., 2021). Two analogous compounds from these families, intrinsic magnetic topological insulator candidates $MnBi_4Te_7$ and $MnSb_4Te_7$ (m=1 and n=1) are sister compounds with the same tetradymite-like crystal structures at ambient conditions (Pei et al., 2022). $MnSb_4Te_7$ is a recently identified ternary compound in the MnTe-$Sb_2Te_3$ quasi-binary system, melting by a peritectic reaction at 901 K (628 °C) (Orujlu et al., 2021). Unlike $MnSb_2Te_4$ from the same quasi-binary system, two surface terminations exist in $MnSb_4Te_7$ along the crystallographic c axis, namely septuple layer and quintuple layer terminations, which may possess different topological surface states (Lin et al., 2024). Upon 0.3 per formula unit of electron doping, magnetic anisotropy energy of $MnSb_4Te_7$ is predicted to reach a very large value of 0.44 meV per formula unit, making it to fulfill the requirement for spintronic applications (Lin et al., 2022). In agreement with first-principles calculations, magnetic phase transition from AFM to FM ordering can be induced with pressure in $MnSb_4Te_7$ (Gao et al., 2023). Therefore, as alignments of opposite magnetic moments through AFM to FM transition can happen with pressure rather than magnetic field, realization of QAHE in $MnSb_4Te_7$ seems possible, paving the way for the possibility of its application in next-generation spintronic devices (Gao et al., 2023). Theoretical calculations predicted that $MnSb_4Te_7$ is a 3D AFM topological insulator in its AFM ground state, however, it can be driven to a FM axion insulator state due to the weak interlayer exchange coupling arising from addition of a quintuple layer of $Sb_2Te_3$, which also results in a lower magnetic transition temperature for $MnSb_4Te_7$, compared to $MnSb_2Te_4$ (Lin et al., 2024). APRES measurements had revealed that the A-type AFM $MnSb_4Te_7$ is a topological insulator that can become an axion insulator protected by inversion symmetry when converted into FM state with a small magnetic field along the c axis (Huan et al., 2021). Interestingly, as a precursor for probing topological superconductivity, superconductivity with a dome-shape phase diagram can be induced with pressure in $MnSb_4Te_7$, which reaches a maximum value of $T_C$=2.2 K at 50.7 GPa, possibly resulting from structural transition to a simple cubic phase and suppression of AFM ordering due to applied pressure (Pei et al., 2022). Another structurally identical, but nonmagnetic compound, $GeSb_4Te_7$, is also a topological insulator confirmed with predictions and ARPES measurements, showing pressure-induced superconductivity, which starts to appear at 11 GPa and reaching a relatively higher maximum value of temperature or $T_C$=8 K with a relatively lower value of applied pressure or 34 GPa compared to $MnSb_4Te_7$ (Zhou et al., 2023).

The comparable ionic radii of $Mn^{2+}$ and $Ge^{2+}$ provide a basis for expecting the formation of homogenous solid solutions through Mn-Ge substitutions over a wide composition range in the $GeSb_4Te_7$–$MnSb_4Te_7$ system. Though magnetic properties can be affected by the decreased Mn content, they can be sacrificed for stability and ease of preparation of $GeSb_4Te_7$ to explore for enhanced magnetotransport properties, topological surface states, and superconductivity besides probing for existence of topological superconductivity. Given the aforementioned considerations, the current study focuses on the preparation of solid solutions along the $GeSb_4Te_7$ – $MnSb_4Te_7$ system and the study of magnetic properties of the $Mn_{0.5}Ge_{0.5}Sb_4Te_7$ solid solution.

# 2 Experimental Details

## 2.1 Synthesis

The polycrystalline samples of the $Mn_xGe_{1-x}Sb_4Te_7$ (MGST-147) series of solid solutions (x = 0, 0.1, 0.3, 0.5, 0.7, 0.9, and 1.0), with varying Mn substitution, were synthesized via high-temperature solid-state reactions using pre-synthesized and homogenized binary compounds: MnTe, GeTe, and $Sb_2Te_3$. High-purity elemental Mn, Ge, Sb, and Te ($\geq$ 99.999 wt %) were initially used as starting materials for the synthesis of the binary compounds. Before the synthesis of MnTe, manganese pieces were treated in nitric acid for a few seconds to remove surface oxide impurities. The stoichiometric amounts of the elements were precisely weighed using an analytical balance with an accuracy of $\pm 5 \times 10^{-5}$ g. To prevent the reaction taking place between manganese and quartz at elevated temperatures during the synthesis of manganese telluride, Mn and Te pieces were placed in a glassy carbon crucible (Orujlu et al., 2021; She et al., 2018; Mammadov et al., 2022; Izzatli et al., 2025), which was then sealed within a quartz tube. The synthesis was conducted in a Thermo Scientific muffle furnace provided with a PID temperature controller for precise regulation of temperature. The heating was performed at a ramp rate of 7.5 K/min with a final temperature set to 50 K above the melting point of each binary compound, as determined from the respective T–x phase diagrams (Mamontov, 1996; Bletskan, 2005; Solé et al., 2022). The quartz tubes were kept at the corresponding temperatures for 3 hours while shaking them occasionally and finally cooled down to the room temperature by switching off the furnace. At the end of the cooling process, the quartz tubes were placed in an annealing oven for one week to achieve homogenization of the synthesized binaries.

Following identification of their single-phase purity by differential thermal analysis (DTA) and powder X-ray diffraction (PXRD) methods, the obtained binary compounds were used to prepare $Mn_xGe_{1-x}Sb_4Te_7$ solid solutions with Mn substitution levels of x = 0, 0.1, 0.2, 0.3, 0.4, 0.5, 0.7, 0.9, and 1.0. For co-melting, the quartz ampoules were first heated to 973 K and held at this temperature for 3 hours to achieve the total dissolution of solid MnTe and GeTe binaries within the melt of $Sb_2Te_3$. Afterwards, the temperature was raised to 1275 K and maintained at this temperature for 3 hours. Unlike conventional bulk crystalline phases, vdW-type phases obtained through the normal melt crystallization show negligible alteration under subsequent thermal treatment because interlayer diffusion is extremely limited (Hasanova et al., 2022; Nabiyev et al., 2025). Therefore, the samples were quenched directly from the melt at the final temperature of 1275 K to preserve phase homogeneity. The quenched samples were subsequently annealed at 725 K for one month to ensure thermodynamic equilibrium. The long-term annealing was used to enhance the quality of crystals through reducing defects and dislocations, which is critical in maintaining the unique electronic properties of topological insulators. At the end of the annealing, the obtained ingots were divided into several pieces for further analysis.

## 2.2 Experimental methods

Structural analyses at room temperature were performed by PXRD with a Bruker D2 Phaser diffractometer employing Cu K$\alpha$ radiation ($\lambda$ = 1.54184 Å) and a LYNXEYE_2 1D detector in Bragg-Brentano configuration. Diffraction data were collected over a $2\theta$ range of 5°-80°. The obtained diffraction patterns were indexed using the reference patterns provided in COD and PDF-4+ databases. The effect of Mn substitution on the lattice parameters was studied through Le Bail analysis in TOPAS software.

The small piece of the polycrystalline ingot was used for DC bulk magnetization measurements. Temperature- and field-dependent magnetization measurements were performed using a commercial superconducting quantum interference device equipped with a vibrating sample magnetometer (SQUID-VSM, MPMS3 by Quantum Design) over the temperature range of 2–

300 K and in magnetic fields up to ±7 T. Prior to the experiments, the instrument was calibrated with a Pd standard. The absence of ferromagnetic impurities was verified by the linear paramagnetic response at 300 K, as evidenced by the hysteresis loop from field-dependent magnetization measurements.

# 3 Results and Discussion

## 3.1 Structural analysis

As shown in Figure 1, the basic unit cell of $GeSb_4Te_7$ / $MnSb_4Te_7$ consists of septuple layers of $GeSb_2Te_4$ / $MnSb_2Te_4$ and quintuple layers of $Sb_2Te_3$ stacking alternately along the c axis leading to a repeating unit of 12 atoms known as SL/QL superlattice. Existence of Dirac cone was predicted only in septuple layer termination though it has not been possible to distinguish between these two terminations in ARPES measurements, possibly due to their very similar band structures (Huan et al., 2021). $GeSb_4Te_7$ / $MnSb_4Te_7$ crystallizes in a rhombohedral structure with $P\bar{3}m1$ (No. 164) space group at ambient conditions and possesses intralayer covalent bonds within both septuple and quintuple layers, and interlayer vdW gaps between them. The weakness of vdW interactions between septuple and quintuple layers is weak, which is useful when it comes to applying large stress and investigating compressive strain effects along the c axis (Lin et al., 2022).

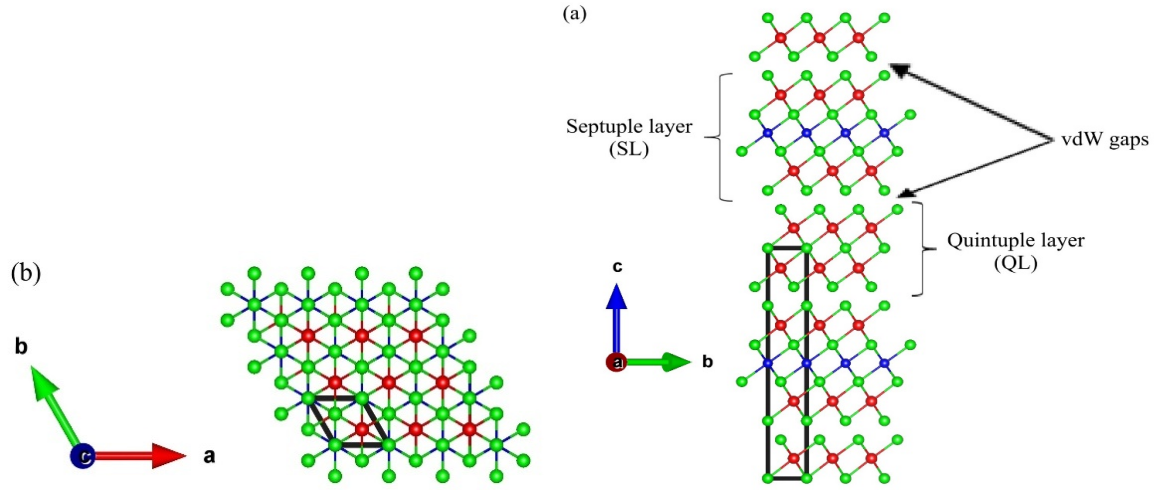


**Figure 1:** Crystal structure of the parent compound $GeSb_4Te_7$ / $MnSb_4Te_7$ with the unit cell highlighted in black. Ge / Mn, Sb, and Te atoms are shown as blue, red, and green spheres, respectively. Panel (a) presents the hexagonal (in-plane) view, while panel (b) displays the rhombohedral (out-of-plane) view.

PXRD patterns for the $Mn_xGe_{1-x}Sb_4Te_7$ solid solutions with different compositions (x = 0 to 1) along the $GeSb_4Te_7$– $MnSb_4Te_7$ system are shown in Figure 2.

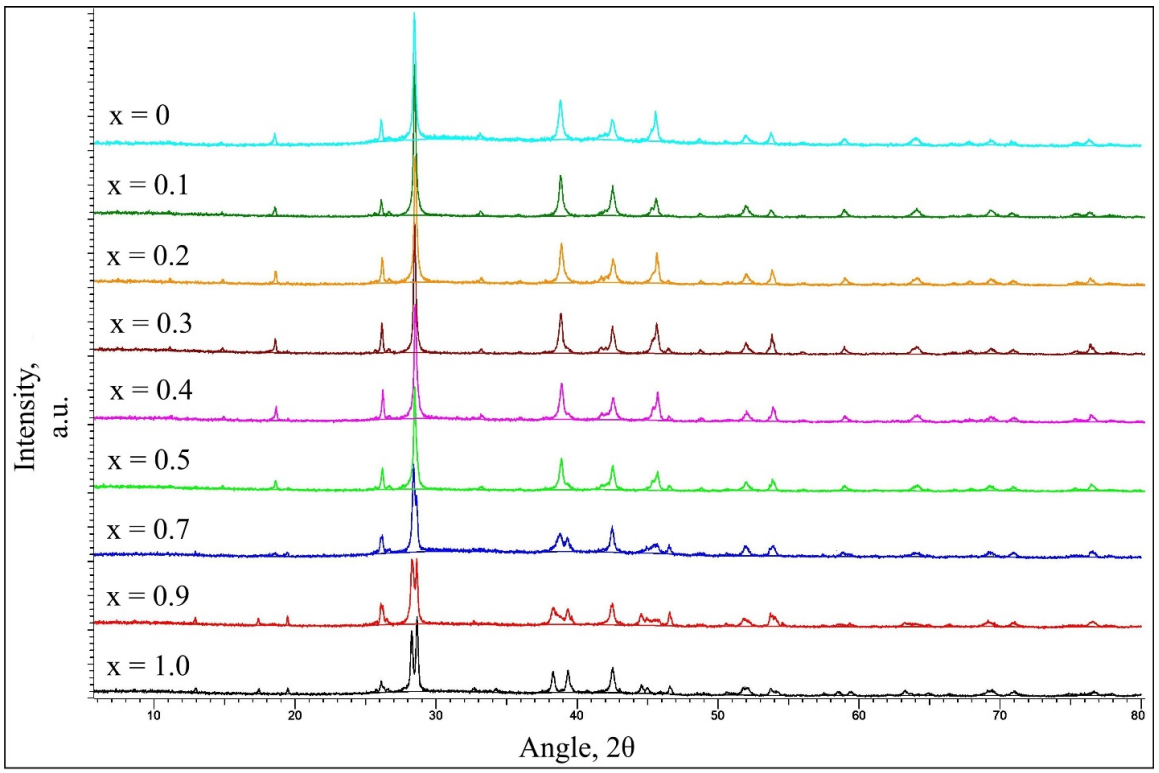


**Figure 2:** PXRD patterns of the alloys along the $GeSb_4Te_7$ – $MnSb_4Te_7$ system with varying Mn content(x), recorded at room temperature over the angle range of $2\theta$ = 5 to 80°. The intensity is given in arbitrary units (a.u.).

As can be seen, all samples with x ≤ 0.5 have almost the same diffraction patterns, all being identical to that of the pristine $GeSb_4Te_7$ with x = 0. This indicates the formation of a continuous solid solution region within this composition range, signifying single-phase purity and homogeneity in this range. The repeated synthesis trials for corresponding compositions under identical preparation conditions produce almost identical diffraction patterns, confirming the stability of the formed phases. As an example, the analyzed PXRD pattern of the solid solution with a composition of $Mn_{0.3}Ge_{0.7}Sb_4Te_7$ is presented in Figure 3a. It is evident that diffraction pattern of this solid solution is monophasic and well indexed with a reference pattern of $GeSb_4Te_7$ from the PDF-4+ database. However, in the x > 0.5 composition range, PXRD patterns of alloys exhibit peak splitting for the highest-intensity peak between $2\theta$ of 28° and 29°, and also for the second highest-intensity peak between $2\theta$ of 38° and 40°, indicating the formation of multiphasic mixture. It appears that under the aforementioned synthesis and thermal treatment conditions, the pure $MnSb_4Te_7$ phase could not be obtained. Similarly, the alloys with compositions $Mn_{0.7}Ge_{0.3}Sb_4Te_7$ and $Mn_{0.9}Ge_{0.1}Sb_4Te_7$ consist of multiphase mixtures, primarily including $GeSb_4Te_7$, $MnSb_2Te_4$, and $Sb_2Te_3$. The PXRD pattern of the $Mn_{0.7}Ge_{0.3}Sb_4Te_7$ sample can be indexed consistently with reference patterns of $GeSb_4Te_7$, $MnSb_2Te_4$, and $Sb_2Te_3$ from the COD and PDF-4+ databases, as depicted in Figure 3b. Failure in obtaining these two compositions and pristine $MnSb_4Te_7$ in single-phase, homogenous form may be attributed to the technical difficulty in stabilizing the Mn-rich compositions. In future studies, the synthesis conditions and thermal treatment parameters will be systematically varied and optimized to achieve single-phase alloys with compositions of x = 0.7, 0.9, and 1. Moreover, other preparation methods may be adopted to increase the solubility range if the aforementioned optimization fails to be satisfactory in terms of obtaining the desired results.

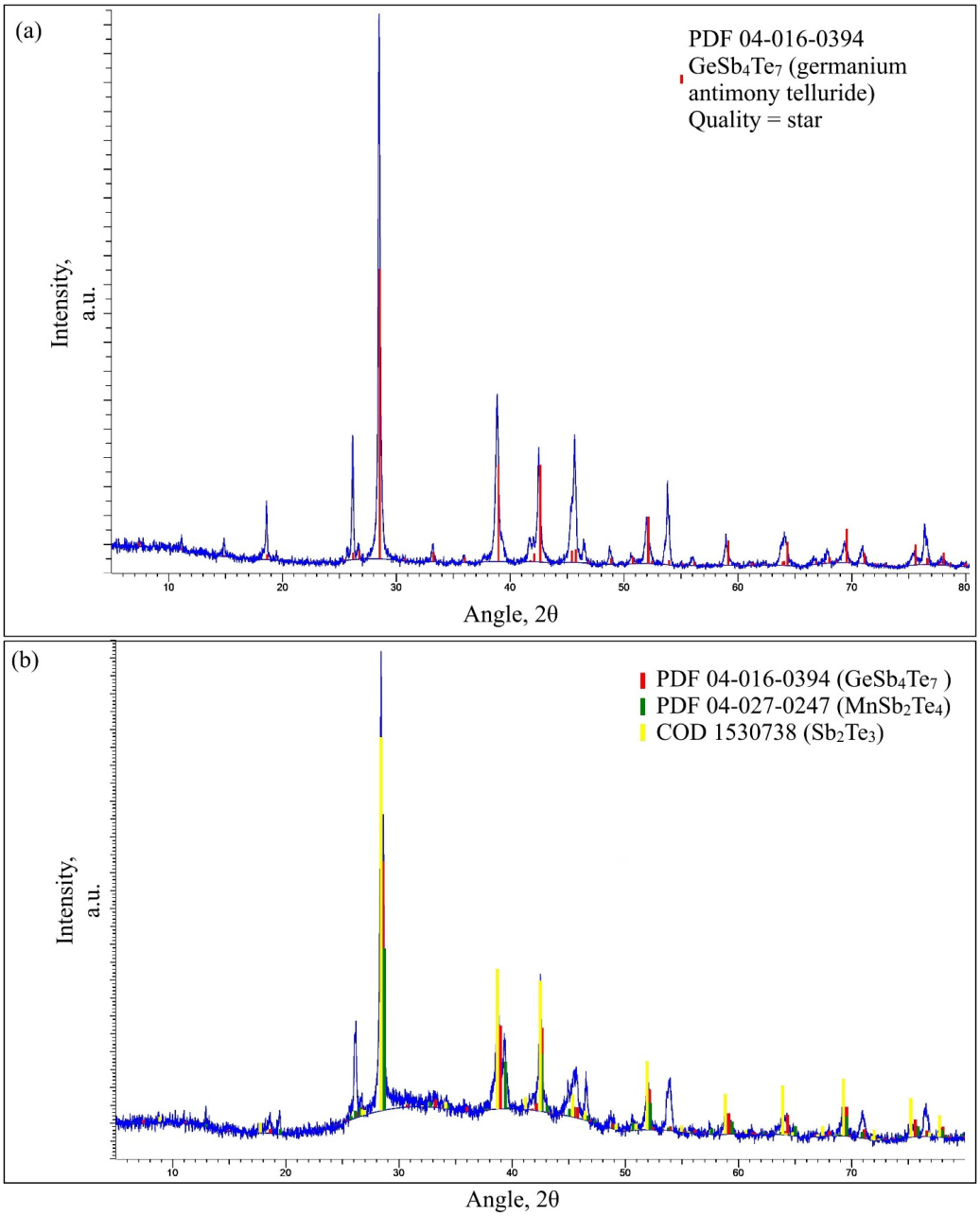


**Figure 3:** PXRD patterns of the alloys with: (a) $Mn_{0.3}Ge_{0.7}Sb_4Te_7$ and (b) $Mn_{0.7}Ge_{0.3}Sb_4Te_7$ compositions.

As $Mn^{2+}$ has a larger ionic size than $Ge^{2+}$, Mn substitution at Ge sites in $GeSb_4Te_7$ is expected to result in lattice expansion and hence increase in lattice parameters. As can be seen in Figure 4, lattice parameter $a$ as a function of Mn substitution (x) exhibits an increasing and almost linear trend, in accordance with the expectation from the aforementioned size factor. Although the lattice parameter $c$ exhibited an almost linear trend decreasing with increased Mn substitution, contrary to the expected expansion. This anomalous behavior of the lattice parameter $c$ as a function of Mn substitution has also been reported recently in the related Bi-based sister system, $GeBi_4Te_7$– $MnBi_4Te_7$ (Buschow & de Boer, 2003). The results of the Le Bail analysis, along with the goodness-of-fit parameters, are indicated in Figures S1.1-S1.6.

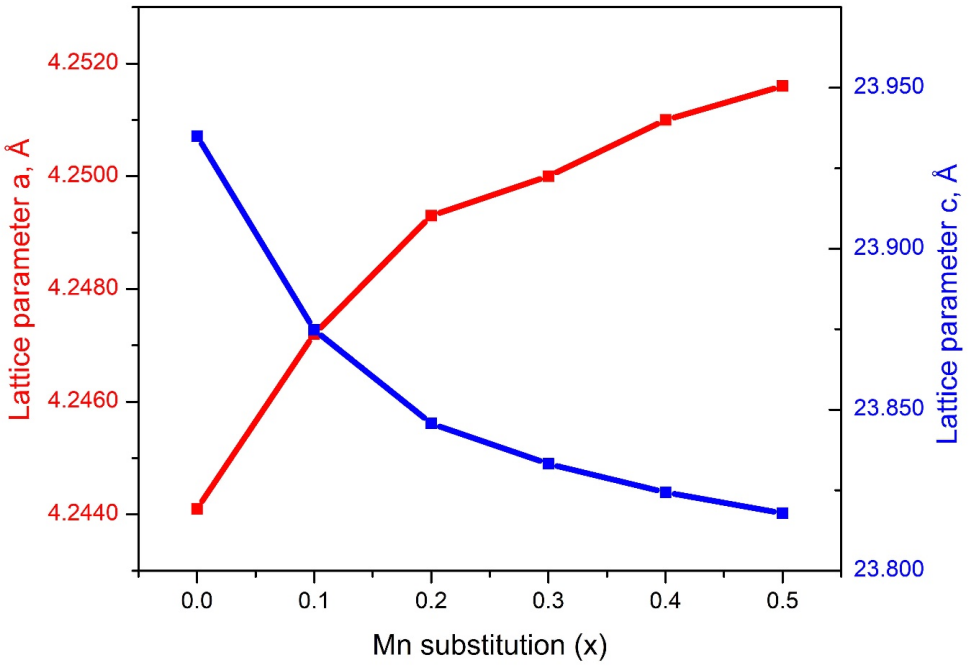


**Figure 4:** Lattice parameters of the MGST-147 solid solutions as a function of Mn substitution ($x$). Lattice parameters are reported in ångströms (Å).

### 3.2 Magnetic properties of the $Mn_{0.5}Ge_{0.5}Sb_4Te_7$ solid solution

$MnSb_4Te_7$ single crystals grown via the flux method had been found to be antiferromagnetic with a Neel temperature of $T_N$ = 13.5 K (Huan et al., 2021) or 14.1 K (Pei et al., 2022). With crystallographic c axis being as the magnetic easy axis, $MnSb_4Te_7$ has intralayer ferromagnetic coupling within septuple layers and interlayer AFM coupling between septuple layers, establishing the overall A-type AFM ordering (Huan et al., 2021; Eremeev et al., 2021). Our measurements on MGST-147 solutions with 10 % and 30 % Mn substitutions exhibited only paramagnetism with no low-temperature magnetic transitions. However, the temperature-dependent molar susceptibility curves in Figure 5 indicate a clear divergence between zero-field cooled (ZFC) and field cooled (FC) runs for the MGST-147 sample with 50 % Mn substitution, signifying the emergence of ferromagnetic-like behavior at low temperatures. The absence of a low-temperature cusp, together with the gradual decrease in molar susceptibility, confirms that antiferromagnetic interactions are not dominant in the solid solution. The dramatic increase in molar susceptibility observed in the FC run arises from the alignment of magnetic moments as the temperature decreases through the magnetic transition temperature under an applied external magnetic field. Furthermore, the presence of very negligible hysteresis loops in the low-temperature, field-dependent magnetization isotherms (Figure 8) provides a strong basis to the claim that the sample is dominantly ferrimagnetic rather than ferromagnetic. Interestingly, the first derivative of the molar susceptibility with respect to temperature revealed two distinct magnetic transitions at low temperatures, occurring at 14.4 K and 3.6 K. Notably, both transitions appeared at the same temperatures in the ZFC and FC runs. The first magnetic transition corresponds to a change from paramagnetic to ferrimagnetic behavior, while the second metamagnetic transition is likely associated with evolution from ferrimagnetic to ferromagnetic ordering. The SQUID magnetometer (MPMS) is capable of measuring extremely small magnetic moments with very high sensitivity (typically on the order of $10^{-8}$ emu, leading

to an error bar less than 1%, with background signal that can be controlled to within 0.1-1% of the total signal). Even when the maximum error of 1 % is taken into account, it does not affect the visibility of the magnetic transition. Similar to the high-temperature transition, both the ZFC and FC runs reveal this low-temperature transition across many samples, confirming its reproducibility and robustness.

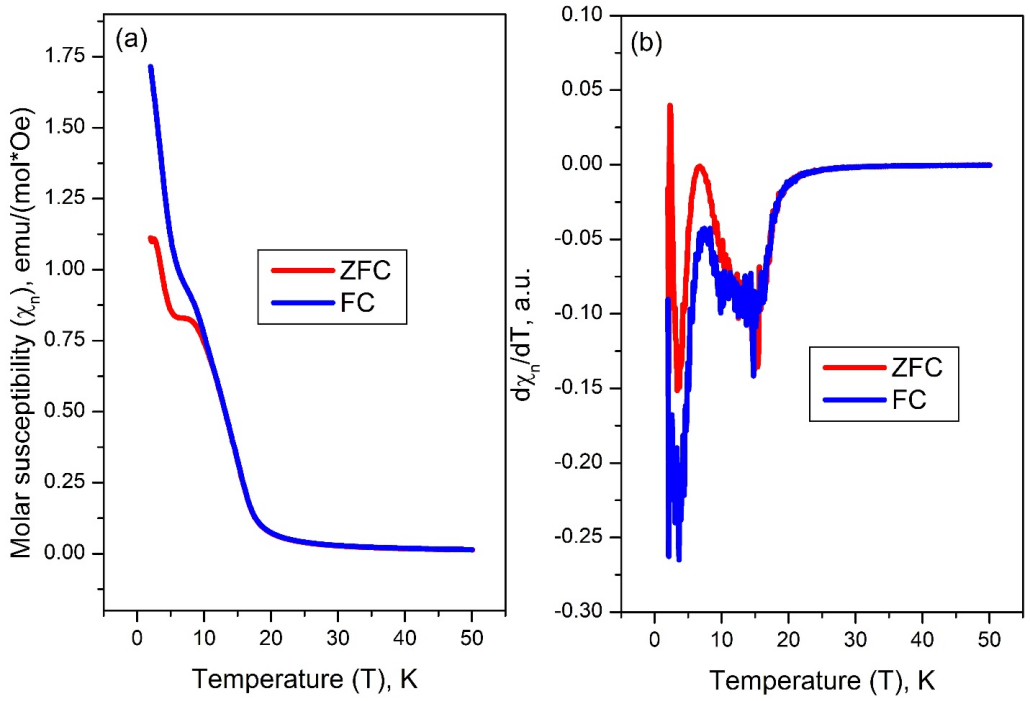


**Figure 5:** (a) ZFC and FC temperature-dependent molar susceptibility curves of the $Mn_{0.5}Ge_{0.5}Sb_4Te_7$ solid solution, given in the partial range from 2 K to 50 K. (b) temperature dependence of the first derivative of the molar susceptibility with respect to temperature. Molar susceptibility is expressed in emu/(mol·Oe), derivative in arbitrary units (a.u.), and temperature in Kelvin (K).

To fit the ZFC and FC inverse molar susceptibility versus temperature data, modified Curie-Weiss law was used by taking into account the temperature-independent molar susceptibility term, $\chi_0$ (emu/(mol·Oe), which can originate from core diamagnetism or Pauli paramagnetism:

$$\chi_n = \chi_0 + \frac{C}{T - T_\theta}$$

Where, $C$ is the Curie constant given in (emu·K)/(mol·Oe) and $T_\theta$ is the Weiss temperature expressed in K. The formula was rearranged to obtain a linear equation of $(\chi_n - \chi_0)^{-1} = a \cdot T + b$, where $a = 1/C$ and $b = -T_\theta/C$.

Fitting of the ZFC experimental data with the modified Curie-Weiss law from 73 K to 300 K is shown in Figure 6, while the residual inverse molar susceptibility, which is the difference between the experimental and fitting values of the ZFC inverse molar susceptibility, as a function of temperature is indicated in Figure S2. The fitting gives a Curie constant of 0.574 (emu·K)/(mol·Oe) and the Weiss temperature of 9.73 K for the ZFC run, and 0.592 (emu·K)/(mol·Oe) and 7.47 K for the FC run (not shown here). The Weiss temperature is positive for both the ZFC and FC data, confirming that magnetic behavior is ferromagnetic-like (ferromagnetic or ferrimagnetic). From the point of view of inverse molar susceptibility versus temperature plot, which is a reliable

guide for magnetic ordering analysis, one clearly sees the downturn near $T_C$ that approaches zero, a clear signature of ferrimagnatism, not observable for other magnetic orderings (Buschow & de Boer, 2003; Mugiraneza & Hallas, 2022). In conformity with this, the Curie-Weiss law follows the relation for a ferrimagnet with a high-temperature linear dependence, and positive T-axis and negative y-axis intercepts, leading to a positive Weiss temperature expected for ferrimagnetic ordering. The effective magnetic moment in $\mu_B$ was calculated using the Curie constant through the formula $\mu_{eff} = \sqrt{8 \cdot C}$ and determined to be 2.20 $\mu_B$ for the ZFC run and 2.26 $\mu_B$ for the FC run. The determined values of the effective moment fall short of the value of 5.92 $\mu_B$ theoretically predicted for $Mn^{2+}$ ions in the high spin state. The lower values are obtained owing to the fact that Mn ions don't exclusively occupy Mn sites, but share the position almost equally with Ge ions as a result of substitution, consequently leading to the significant reduction of the effective moment. Although the reduction of the effective moment can arise primarily from magnetic dilution (Frolov et al., 2024; Qian et al., 2022), the possible contributions from enhanced Mn–Te/Ge hybridization (Frolov et al., 2024; Estyunina et al., 2023) can also play a role in partially delocalizing Mn 3d electrons.

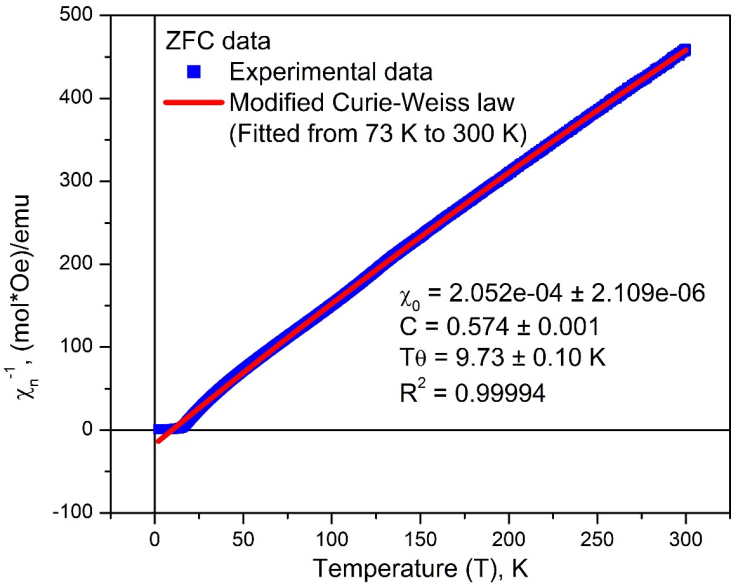


**Figure 6:** ZFC inverse molar susceptibility versus temperature data fitted with modified Curie-Weiss law. The inverse molar susceptibility is given in (mol·Oe)/emu, while temperature is expressed in Kelvin (K). The extracted parameters, along with the fit quality value are also depicted.

The field-dependent magnetization isotherms indicated in Figure 7 exhibit a nonlinear, saturating behavior of magnetization as a function of magnetic field strength both slightly above and below the first transition temperature of 14.4 K, with isotherms below this temperature showing more pronounced saturation. The saturation magnetizations measured at 2, 5, and 10 K were determined to be 0.50, 0.49, and 0.45 $\mu$B/f.u., respectively, corresponding to approximately one-fourth of the saturation magnetic moment reported for the pristine $MnSb_4Te_7$ (Huan et al., 2021). Although 50 % Mn substitution replaces half of the Ge ions, the saturation magnetic moment decreases by a factor of about four, possibly due to the combined effect of magnetic dilution as a result of Ge ions and the presence of Mn ions at Sb sites in both septuple and quintuple layers, which had been reported for Sb-doped $MnBi_4Te_7$ (Yan et al., 2023).

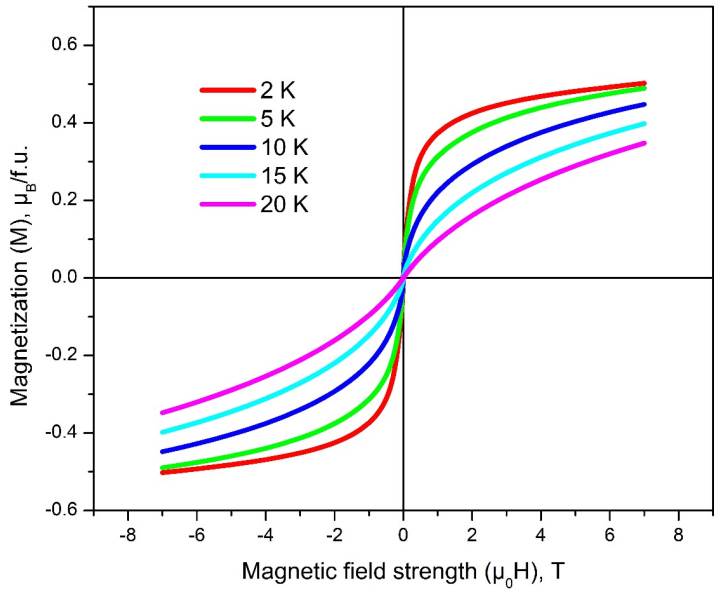


**Figure 7:** Field-dependent magnetization isotherms at different temperatures for the $Mn_{0.5}Ge_{0.5}Sb_4Te_7$ solid solution. Magnetization is given in Bohr magnetons per formula unit ($\mu_B$/f.u.), while magnetic field strength is expressed in tesla (T).

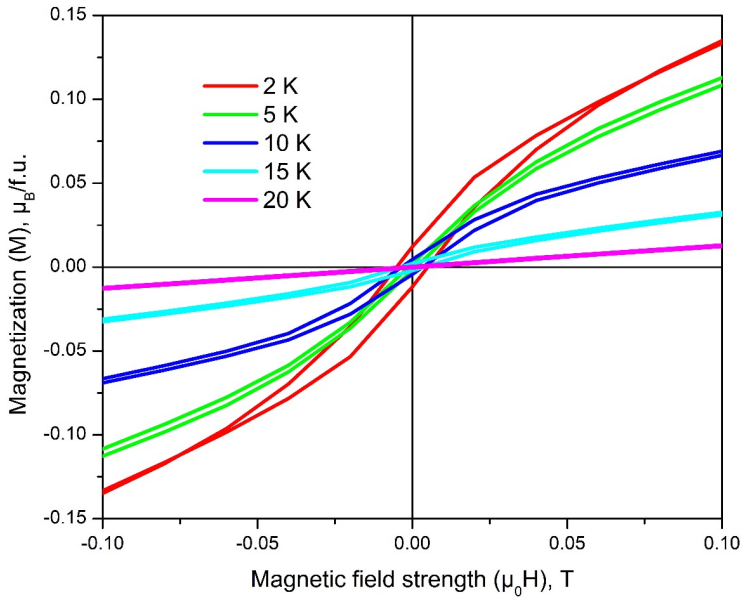


**Figure 8:** The enlarged view of the field-dependent magnetization isotherms at different temperatures for the $Mn_{0.5}Ge_{0.5}Sb_4Te_7$ solid solution.

Theoretical calculations had revealed that Mn ions in $MnSb_4Te_7$ couple ferromagnetically within the septuple layers, while the interlayer coupling between the septuple layers is antiferromagnetic (Eremeev et al., 2021). However, due to the presence of Ge ions that exist between Mn ions at Mn sites, intralayer distance between Mn ions is considerably larger compared to the same

distance in $MnSb_4Te_7$. The increased distance causes suppression of intralayer ferromagnetic interactions and enhances intralayer antiferromagnetic interactions, leading to a compensation effect and hence the decrease of the saturation magnetic moment. Moreover, the site mixing may also lead to antiferromagnetic coupling of Mn ions at Mn sites to those at Sb sites, resulting in compensation effect and hence the greatly reduced saturated magnetic moment (Yan et al., 2023).

The Figure 8 depicts the enlarged view of the magnetization versus magnetic field plot from Figure 7, indicating the presence of very negligible hysteresis loops and hence the dominant ferrimagnetic behavior. This close view reveals that existence of a hysteresis loop can confidently be claimed to take place at 2 K below the second magnetic transition and confirms that this transition corresponds to a metamagnetic shift from ferrimagnetic to ferromagnetic behavior. However, for higher temperatures, hysteresis loop is either very negligible or nonexistent, signifying a dominant ferrimagnetic behavior. In addition, the absence of any spin-flop transitions, along with the nonzero values of the magnetization at very low magnetic fields suggest that antiferromagnetic interactions are not dominant in the sample.

# 4 Conclusion

The structural analyses of the polycrystalline samples prepared along the $GeSb_4Te_7$-$MnSb_4Te_7$ system were carried out with PXRD and Le Bail analysis, while the magnetic properties of the MGST-147 solid solution with 50 % Mn substitution were studied with SQUID magnetometry. PXRD measurements and analyses showed that at given conditions, maximum of 50 % solubility was achieved. In other words, the alloys $Mn_xGe_{1-x}Sb_4Te_7$ (MGST-147) with $x \leq 0.5$ are homogeneous, while the alloys with $x > 0.5$ are heterogeneous, consisting of a mixture of two or more phases. Le Bail analysis revealed that the lattice parameter $a$ increases almost linearly with increasing Mn content, in accordance with the larger ionic size of $Mn^{2+}$. By contrast, the lattice parameter $c$ exhibited a decreasing linear trend, contrary to the expected increasing linear trend. This unexpected behavior has recently been reported for the sister system with Bi besides the current system with Sb. Unlike the antiferromagnetic pristine $MnSb_4Te_7$, magnetic measurements on the MGST-147 solid solution with 50 % Mn substitution uncovered two distinct magnetic transitions at 14.4 K and 3.6 K that correspond to paramagnetic-to-ferrimagnetic and ferrimagnetic-to-ferromagnetic transitions, respectively. Compared to the pristine $MnSb_4Te_7$, effective moment and saturation magnetic moment decreased significantly in the 50 % Mn-substituted sample. The large decrease for the value of the former originates from the joint action of the magnetic dilution due to presence of Ge ions and Mn-Te/Ge hybridization. The significant reduction in the value of the latter can be attributed to the combined effect of magnetic dilution and the presence of Mn ions at Sb sites in both septuple and quintuple layers, both leading to intralayer AFM coupling between Mn ions at Mn sites, and also between Mn ions at Mn sites and those at Sb sites. This study provides a starting point for currently ongoing investigations, in which attempts are being made to increase the solubility range within the system and a detailed study on the microstructure and composition analysis is planned to be performed for the entire composition range to further confirm the phase stability and homogeneity.

**Acknowledgements**

Authors wish to thank Jerome Robert for help with magnetic measurements and Bohdan Kundys for useful comments on the manuscript.

## References


Bletskan, D. I. (2005). Phase Equilibrium in the Systems AIV–BVI. *J. Ovonic Res.,* 1, 53-60.

Buschow, K.H.J., de Boer, F.R. (2003). The magnetically ordered state. In *Physics of Magnetism and Magnetic Materials* (pp. 19-42). Boston, MA: Springer US. https://doi.org/10.1007/0-306-48408-0_4.

Chang, C. Z., Zhang, J., Feng, X., Shen, J., Zhang, Z., Guo, M., ... & Xue, Q. K. (2013). Experimental observation of the quantum anomalous Hall effect in a magnetic topological insulator. *Science, 340*(6129), 167-170. ttps://doi.org/10.1126/science.1234414.

Deng, Y., Yu, Y., Shi, M. Z., Guo, Z., Xu, Z., Wang, J., ... & Zhang, Y. (2020). Quantum anomalous Hall effect in intrinsic magnetic topological insulator $MnBi_2Te_4$. *Science, 367*(6480), 895-900. https://doi.org/10.1126/science.aax8156.

Eremeev, S. V., Rusinov, I. P., Koroteev, Y. M., Vyazovskaya, A. Y., Hoffmann, M., Echenique, P. M., ... & Chulkov, E. V. (2021). Topological magnetic materials of the $(MnSb_2Te_4)\Delta(Sb_2Te_3)$ n van der Waals compounds family. *The Journal of Physical Chemistry Letters, 12*(17), 4268-4277. https://doi.org/10.1021/acs.jpclett.1c00875.

Estyunina, T. P., Shikin, A. M., Estyunin, D. A., Eryzhenkov, A. V., Klimovskikh, I. I., Bokai, K. A., ... & Tarasov, A. V. (2023). Evolution of $Mn_{1-x}Ge_xBi_2Te_4$ Electronic Structure under Variation of Ge Content. *Nanomaterials, 13*(14), 2151. https://doi.org/10.3390/nano13142151.

Frolov, A. S., Usachov, D. Y., Tarasov, A. V., Fedorov, A. V., Bokai, K. A., Klimovskikh, I., ... & Yashina, L. V. (2024). Magnetic dirac semimetal state of (Mn, Ge) $Bi_2Te_4$. *Communications Physics, 7*(1), 180. https://doi.org/10.1038/s42005-024-01675-w.

Gao, L., Wu, J., Xi, M., Pei, C., Wang, Q., Zhao, Y., ... & Qi, Y. (2023). Pressure-tunable magnetic topological phases in magnetic topological insulator $MnSb_4Te_7$. *Applied Physics Letters, 122*(17). https://doi.org/10.1063/5.0146605.

Geim, A.K., Grigorieva, I.V. (2013). Van der Waals heterostructures. *Nature, 499*(7459), 419-425. https://doi.org/10.1038/nature12385.

Hasanova, G. S., Aghazade, A. I., Babanly, D. M., Imamaliyeva, S. Z., Yusibov, Y. A., & Babanly, M. B. (2022). Experimental study of the phase relations and thermodynamic properties of Bi-Se system. *Journal of Thermal Analysis and Calorimetry, 147*(11), 6403-6414. https://doi.org/10.1007/s10973-021-10975-0.

Huan, S., Zhang, S., Jiang, Z., Su, H., Wang, H., Zhang, X., ... & Guo, Y. (2021). Multiple magnetic topological phases in bulk van der Waals crystal MnSb 4 Te 7. *Physical Review Letters, 126*(24), 246601. https://doi.org/10.1103/PhysRevLett.126.246601.

Izzatli, S. B., Orujlu, E. N., Jafarov, Y. I., & Babanly, M. B. (2025). Phase Relations and Tunable Solid Solutions in the Pseudoternary System MnTe–$Sb_2Te_3$–$Bi_2Te_3$. *Journal of Chemical & Engineering Data, 70*(4), 1759-1768. https://doi.org/10.1021/acs.jced.4c00711.

Lin, J. Y., Chen, Z. J., Xie, W. Q., Yang, X. B., & Zhao, Y. J. (2022). Toward ferromagnetic semimetal ground state with multiple Weyl nodes in van der Waals crystal $MnSb_4Te_7$. *New Journal of Physics, 24*(4), 043033. https://doi.org/10.1088/1367-2630/ac6231.

Lin, J. Y., Cao, Z., Chen, Z. J., He, W., Zeng, J., Yang, X. B., ... & Zhao, Y. J. (2024). Topological Crystalline Insulator Phases in Magnetic van der Waals Crystal $MnBi_4Te_7$ and $Mn_2Bi_2Te_5$ Families. *The Journal of Physical Chemistry C, 128*(47), 20451-20458. https://doi.org/10.1021/acs.jpcc.4c05870.

Mammadov, F. M., Niftiev, N. N., Jafarov, Y. I., Babanly, D. M., Bakhtiyarly, I. B., & Babanly, M. B. (2022). Physicochemical Analysis of the MnTe - Ga2Te3 - In2Te3 System and AC Electrical Conductivity of $MnGaInTe_4$. *Russian Journal of Inorganic Chemistry, 67*(10), 1623-1633. https://doi.org/10.1134/S0036023622600769.

Mamontov, M. N. (1996). Optimization of thermodynamic data on liquidus of Mn-Te phase diagram in associated-solution model. *Neorganicheskie Materialy*, 32. https://www.osti.gov/etdeweb/biblio/518952 (accessed October 23, 2024).

Mugiraneza, S., Hallas, A. M. (2022). Tutorial: a beginner's guide to interpreting magnetic susceptibility data with the Curie-Weiss law. *Communications Physics, 5*(1), 95. https://doi.org/10.1038/s42005-022-00853-y.

Nabiyev, E. R., Orujlu, E. N., Babanly, D. M., Imamaliyeva, S. Z., Yusibov, Y. A., & Babanly, M. B. (2025). Standard Thermodynamic Functions of $Sb_2Te_3$-Rich Germanium Antimony Tellurides: EMF Measurements. *International Journal of Thermophysics, 46*(10), 1-15. https://doi.org/10.1007/s10765-025-03631-4.

Novoselov, K. S., Geim, A. K., Morozov, S. V., Jiang, D. E., Zhang, Y., Dubonos, S. V., ... & Firsov, A. A. (2004). Electric field effect in atomically thin carbon films. *Science, 306*(5696), 666-669.

Orujlu, E. N., Aliev, Z. S., Amiraslanov, I. R., & Babanly, M. B. (2021). Phase equilibria of the MnTe-Sb2Te3 system and synthesis of novel ternary layered compound–$MnSb_4Te_7$. *Physics and Chemistry of Solid State, 22*(1), 39-44. https://doi.org/10.15330/pcss.22.1.39-44.

Otrokov, M. M., Klimovskikh, I. I., Bentmann, H., Estyunin, D., Zeugner, A., Aliev, Z. S., ... & Chulkov, E. V. (2019). Prediction and observation of an antiferromagnetic topological insulator. *Nature, 576*(7787), 416-422. https://doi.org/10.1038/s41586-019-1840-9.

Pei, C., Xi, M., Wang, Q., Shi, W., Wu, J., Gao, L., ... & Qi, Y. (2022). Pressure-induced superconductivity in magnetic topological insulator candidate MnSb 4 Te 7. *Physical Review Materials, 6*(10), L101801. https://doi.org/10.1103/PhysRevMaterials.6.L101801.

Qian, T., Yao, Y. T., Hu, C., Feng, E., Cao, H., Mazin, I. I., ... & Ni, N. (2022). Magnetic dilution effect and topological phase transitions in $(Mn_{1-x}Pb_x)Bi_2Te_4$. *Physical Review B, 106*(4), 045121. https://doi.org/10.1103/PhysRevB.106.045121.

She, X., Su, X., Xie, H., Fu, J., Yan, Y., Liu, W., ... & Tang, X. (2018). Ultrafast synthesis and thermoelectric properties of Mn1+ x Te compounds. *ACS Applied Materials & Interfaces, 10*(30), 25519-25528. https://doi.org/10.1021/acsami.8b07255.

Solé, S., Schmetterer, C., & Richter, K. W. (2022). A revision of the Sb-Te binary phase diagram and crystal structure of the modulated $\gamma$-phase field. *Journal of Phase Equilibria and Diffusion, 43*(6), 648-659. https://doi.org/10.1007/s11669-022-00958-5.

Tokura, Y., Yasuda, K., & Tsukazaki, A. (2019). Magnetic topological insulators. *Nature Reviews Physics, 1*(2), 126-143. ttps://doi.org/10.1038/s42254-018-0011-5.

Yan, J. Q., Huang, Z., Wu, W., & May, A. F. (2022). Vapor transport growth of MnBi2Te4 and related compounds. *Journal of Alloys and Compounds*, 906, 164327. https://doi.org/10.1016/j.jallcom.2022.164327.

Yu, R., Zhang, W., Zhang, H. J., Zhang, S. C., Dai, X., & Fang, Z. (2010). Quantized anomalous Hall effect in magnetic topological insulators. *Science, 329*(5987), 61-64. https://doi.org/10.1126/science.1187485.

Zhou, W., Li, B., Shen, Y., Feng, J. J., Xu, C. Q., Guo, H. T., ... & Xu, X. (2023). Multiple superconducting phases driven by pressure in the topological insulator GeSb 4 Te 7. *Physical Review B, 108*(18), 184504. https://doi.org/10.1103/PhysRevB.108.184504.

## SUPPLEMENTARY SECTION

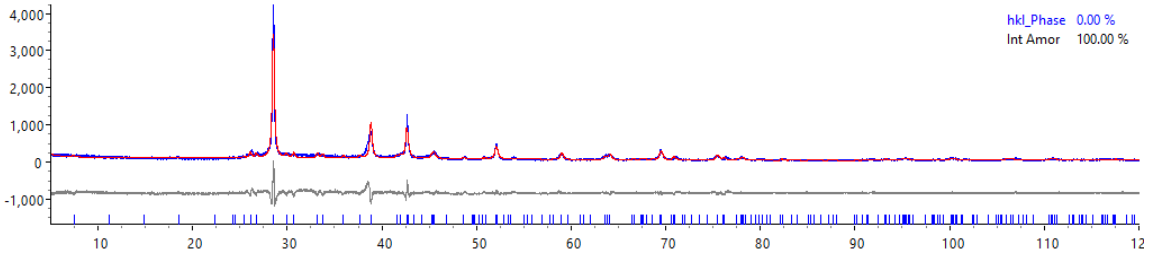


**Figure S1.1.** Le Bail analysis of the x = 0 sample ($R_p$ = 13.45 %, $R_{wp}$ = 16.92 %, $R_{exp}$ = 20.39 %, and GoF = 1.93).

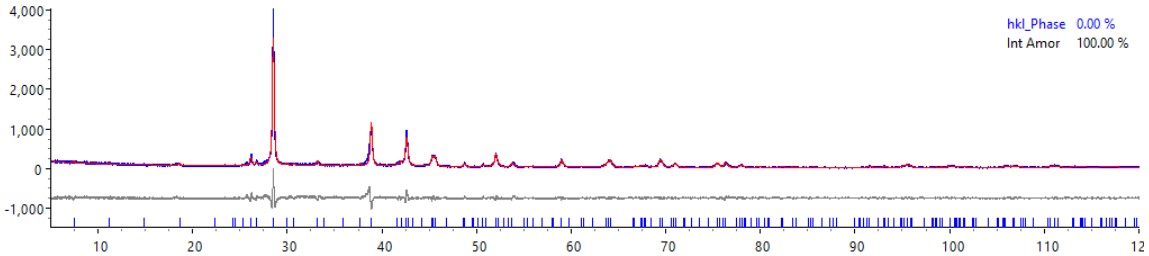


**Figure S1.2.** Le Bail analysis of the x = 0.1 sample ($R_p$ = 12.96 %, $R_{wp}$ = 16.52 %, $R_{exp}$ = 20.08 %, and GoF = 1.19).

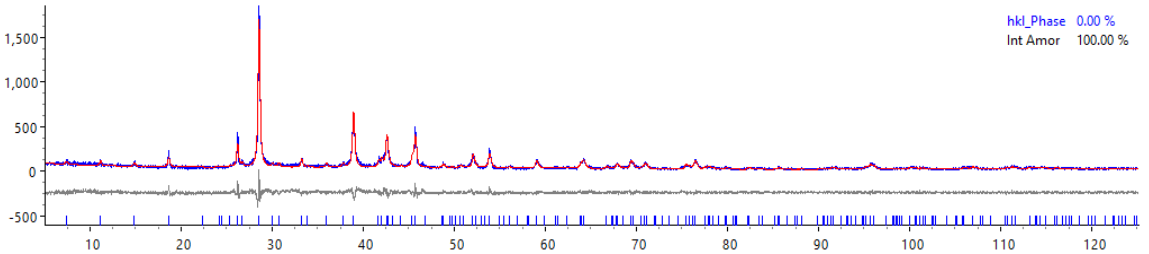


**Figure S1.3.** Le Bail analysis of the x = 0.2 sample ($R_p$ = 12.72 %, $R_{wp}$ = 16.08 %, $R_{exp}$ = 12.51 %, and GoF = 1.29).

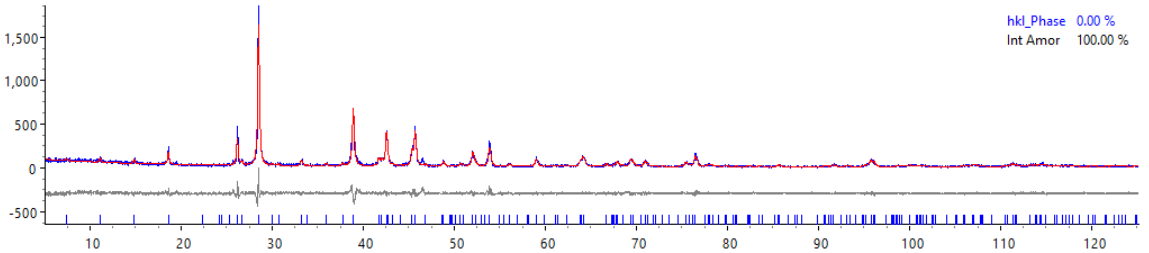


**Figure S1.4.** Le Bail analysis of the x = 0.3 sample ($R_p$ = 13.55 %, $R_{wp}$ = 17.64 %, $R_{exp}$ = 13.92 %, and GoF = 1.27).

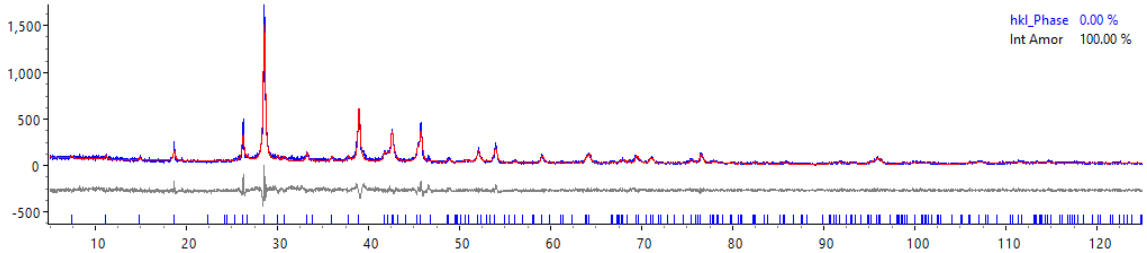


**Figure S1.5.** Le Bail analysis of the x = 0.4 sample ($R_p$ = 13.46 %, $R_{wp}$ = 17.08 %, $R_{exp}$ = 12.58 %, and GoF = 1.36).

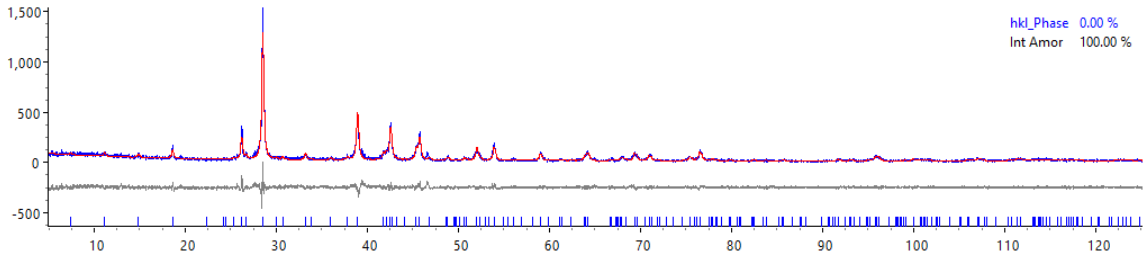


**Figure S1.6.** Le Bail analysis of the x = 0.5 sample ($R_p$ = 13.64 %, $R_{wp}$ = 17.56 %, $R_{exp}$ = 14.12 %, and GoF = 1.24).

**Figure S1.** Le Bail analysis of the solid solutions with different Mn substitutions ($x$). In each figure, the experimental data are shown in blue, the calculated profile in red, and the difference curve in grey. The vertical blue ticks mark the Bragg peak positions of the $GeSb_4Te_7$-type structure crystallizing in the $P\bar{3}m1$ (No. 164) space group.

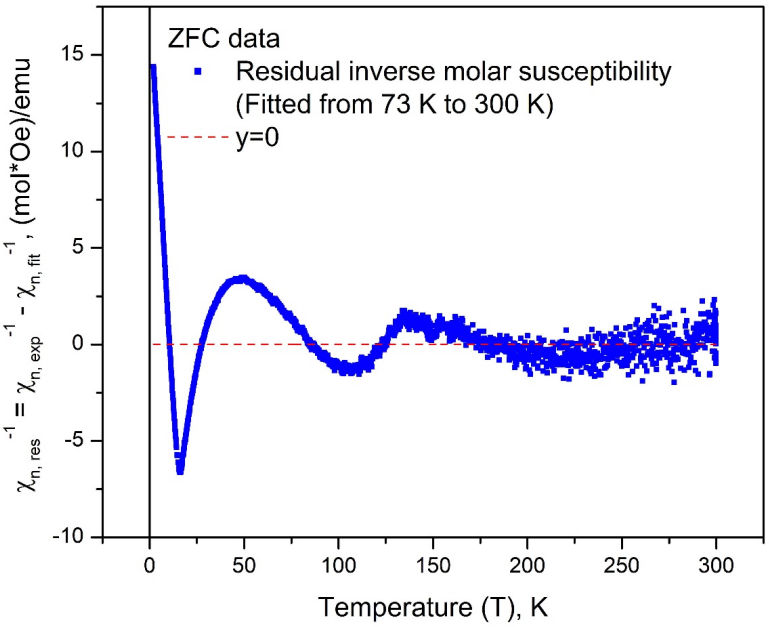


**Figure S2.** ZFC residual inverse molar susceptibility, which is the difference between the experimental and fitting values of the inverse molar susceptibility, as a function of temperature. The residual inverse molar susceptibility is given in (mol·Oe)/emu, while temperature is expressed in Kelvin (K).